Behavior of five-pad tilting–pad journal bearings with different pivot stiffness

Dang Phuoc Vinh[1][0000-0002-9515-5173], Steven Chatterton[2][0000-0003-4170-009X] and Paolo Pennacchi[2][0000-0001-8174-0462]

[1] Dept. of Mechanical Engineering, The University of Danang – Danang University of Science and Technology

[2]Dept. of Mechanical Engineering, Politecnico di Milano, Via G. La Masa 1, 20145 Milan, Italy

dpvinh@dut.udn.vn, {steven.chatterton, paolo.pennacchi}@polimi.it

Abstract. In this paper, two different five-shoe tilting-pad journal bearings, namely rocker-backed pivot and spherical pivot with different pivot stiffness have been characterized with different working conditions. For the spherical pivot bearing, elastic shims and displacement restriction component are introduced to recognize the role of the variable stiffness of pivot. The copper is used for the material of the shim. An analysis of the dynamic behavior of the two bearings using a thermo-elasto-hydrodynamic model is presented first. This model considers the flexibility for both pad as well as pivot and a simple thermal model only for the fluid film temperature to accurately calculate the performance of bearings. The model also accounts for pivot stiffness of pads. The predicted dynamic coefficients of the two bearings were compared with the experimentally measured ones. The results show that the pivot stiffness or the pivot flexibility plays an important role in the dynamic coefficients estimation.

Keywords: tilting-pad journal bearings; pivot stiffness; dynamic characteristics; thermo-elasto-hydrodynamic model; experimental tests.

1 Introduction

Over the years, the topic of pivot flexibility of tilting-pad journal bearings (TPJBs) has become more and more important, especially for the bearings operating with high applied static load and high rotational speed. Studies including flexibility of the pad and the pivot on the modeling in order to obtain accurate results of TPJBs are well documented.

Chen et al. [1] studied numerically the behavior of the tilting-pad journal gas bearings with variable pivot stiffness. Based on their finding, they concluded that compared with the fixed pads, the minimum oil-film thickness increases if flexibility of the pad and the pivot is considered.

In 2013, San Andres and Tao [2] investigated the role of pivot flexibility in TPJBs on the dynamic coefficients. It was found that if pivot stiffness is one order of magnitude larger than the oil film stiffness, the effect of pivot flexibility on the TPJB dynamic coefficients is negligible. Wilkes et al. [3] studied the effects of the pad and pivot flexibility in forecasting the dynamic coefficients for the TPJB. They considered the variations of the bearing clearance with the working temperature and determined

the differences between predicted and measured dynamic coefficients as functions of dynamic excitation. The study on the influence of flexibility of the pad and pivot on the dynamic behaviors of the TPJBs was also carried out [4]-[6].

In this paper, the dynamic characteristics of two different five-shoe TPJB, namely rocker-backed pivots and spherical pivots with different pivot stiffness have been studied by means of a TEHD model. The model accounts for pivot stiffness of pads which are determined by a model based on the Hertz contact theory and the experimental measurements. The pivot stiffness calculation using the experimental measurement is presented. The experimental tests were performed for these two bearings using a suitable test-rig in order to validate the model. The predicted dynamic coefficients of the two bearings were compared with the measured ones.

2 TEHD bearing model

Fig. 1 represents the geometry of a single pad from the five-pad tilting-pad journal bearing, where O_b and O_j is the centre of the bearing and the journal, respectively.

A thorough description of the TEHD model to estimate the static and dynamic behaviors of a five-pad TPJB is provided in [7]-[12].

The hydrodynamic model is based on the well-known Reynolds equation:

$$\begin{aligned}&\frac{\partial}{\partial x}\left(\frac{\rho h^3}{\mu}\frac{\partial p}{\partial x}\right)+\frac{\partial}{\partial z}\left(\frac{\rho h^3}{\mu}\frac{\partial p}{\partial z}\right)\\&=6\left[\left(U_1-U_2\right)\frac{\partial h}{\partial x}+h\frac{\partial}{\partial x}\left(U_1+U_2\right)\right.\\&\left.+\left(W_1-W_2\right)\frac{\partial h}{\partial z}+h\frac{\partial}{\partial z}\left(W_1+W_2\right)+2\left(V_1+V_2\right)\right]\end{aligned}\qquad(1)$$

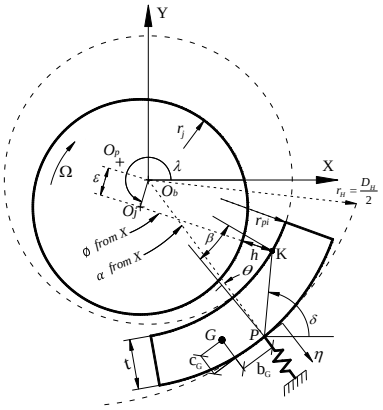

Fig. 1. Sketch of a rocker-backed TPJB [7].

where p is the pressure in the oil-film, h is the oil-film thickness, μ is the dynamic viscosity, ρ is the density of oil, z is the axial direction, x is the tangential direction. The velocity vector component of the shaft and the pads are defined by U_1, V_1, W_1 and U_2, V_2, W_2, respectively.

The effect of temperature on the dynamic viscosity $\mu(T)=\mu_{40°C}\exp\left[\kappa\left(T_{40°C}-T\right)\right]$ and oil density $\rho(T)=\rho_{40°C}\left[1+\alpha_v\left(T_{40°C}-T\right)\right]$ is considered using a simple two-dimensional thermal model, governed, at steady state, by the energy equation:

$$\rho c_p\left(u\frac{\partial T}{\partial x}+w\frac{\partial T}{\partial z}\right)=k_{OIL}\left(\frac{\partial^2 T}{\partial x^2}+\frac{\partial^2 T}{\partial z^2}\right)+\mu\left[\left(\frac{\partial u}{\partial y}\right)^2+\left(\frac{\partial w}{\partial y}\right)^2\right]\qquad(2)$$

where κ is the viscosity index and α_v is the thermal expansion coefficient of the oil, c_p and k_L are the heat capacity and the conductivity of the lubricant respectively.

Equation (2) has been integrated using a finite difference method, where adiabatic conditions at the shaft, pad surfaces and constant oil temperature in the oil film thickness direction are considered.

3 Test-rig and bearing under test

A detail description of the test-rig and a five-pad rocker-backed TPJB is provided in [7] and [12]. In the test rig, the rotor axis can describe orbits similar to the real configuration of a rotating machine in which two identical five-pad TPJBs (in the condition of nominal dimensions) which are labeled as **1** and **2** in Fig. 2 support the shaft. The shaft is driven using a 6.0 kW inverter-driven electric motor by means of a flexible coupling up to the maximum rotational speed of 3000 rpm.

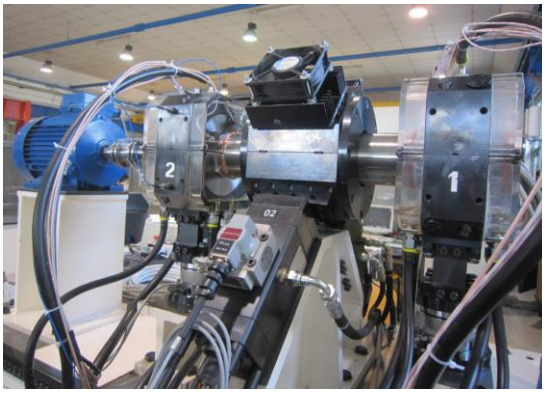

Fig. 2. Test rig for experimental tests [7]

The load is applied in the middle of the shaft by means of two hydraulic actuators arranged in an orthogonal configuration at ±45° with respect to the load cells. The actuators are connected to the shaft by means of two deep-groove high-precision ball bearings. Due to this configuration, a static load, as well as a dynamic load, can be applied in any direction.

a)

b)

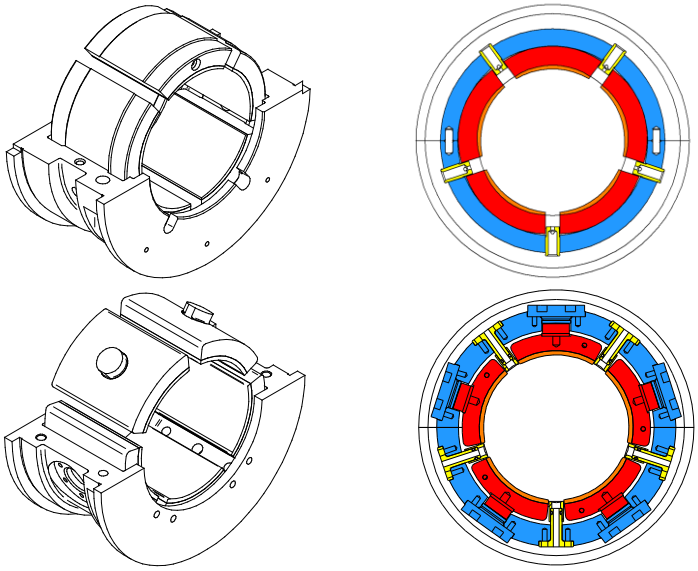

Fig. 3. Five-shoe TPJB under test (a) rocker-backed and (b) spherical pivot

During the tests, the oil inlet was kept at approximately $40 \pm 0.5°C$ using a closed-loop PI. The bearing under test, shown in Fig. 3a, is a five shoe rocker-backed TPJB. The bearing is installed in its housing in a standard LOP configuration with a nominal diameter of 100 mm and a length-to-diameter ratio (L/D) of 0.7.

For the spherical pivot bearing, elastic shims and displacement restriction component are introduced to recognize the role of the variable stiffness of pivot. The material of the shim can be changed to offer different stiffness in the radial direction (see Fig. 3b). In this paper, copper has been used for the shims. The pivot system (including pivot, cap, and shim) is installed on each pad (see Fig. 4).

The rocker-backed bearing and the spherical pivot bearing specifications and operating conditions are listed in Table 1

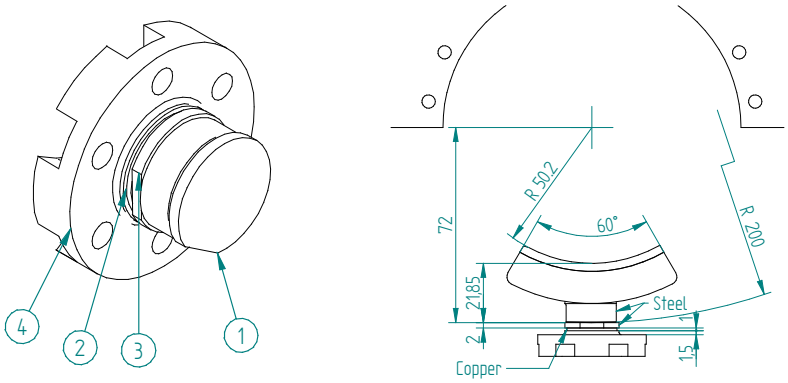

a) **b)**

Fig. 4. (a) 3D drawing of the pivot and (b) drawing of the pad and pivot (nominal dimension). 1: pivot (pad side); 2: copper liner (shim); 3: pivot (housing side); 4: pads cap.

Table 1. Specifications and operating conditions of rocker-backed and spherical pivot bearing.

Item	**Unit**	**Value/Span**	
		Rocker back	**Spherical pivot**
Number of pads		5	5
Configuration w.r.t bearing housing		LOP	LOP
Shaft diameter	mm	99.86	99.86
Bearing length	mm	69.6	75
Housing radius	mm	66	-
Pad outer radius	mm	59.8	-
Radius of pad inner surface	mm	50.06	50.15
Radius of spherical pivot	mm	-	200
Nominal pad thickness	mm	16	-
Nominal pad thickness (pad+pivot)	mm	-	21.85
Angular amplitude of pads	degree	63.5	60
Oil inlet temperature	°C	40	40
Pad mass	kg	0.540	0.823
Pad mass moment of inertia w.r.t pivot	kg m^2	0.256E-3	1.380 E-3

4 Pivot stiffness calculation

Assuming the same material properties for the pad pivot and its contact housing, the pivot stiffness equation considering the contact Hertz theory [13] are given by:

$$K_{\text{rocker backed}} = \frac{\pi EL}{2\left(1-\nu^2\right)}\left(\frac{2}{3}+\ln\frac{\pi EL\left(D_H-D_P\right)}{4W\left(1-\nu^2\right)}\right)$$
$$K_{\text{spherical}} = \frac{W}{\sqrt[3]{\frac{9W^2\left(1-\nu^2\right)^2}{2E^2D_s}}} \tag{3}$$

where E and ν are the Young's modulus and the Poisson coefficient respectively, D_H and D_P are the diameter of the bearing housing and pivot respectively, D_s is the diameter of spherical pivot, and W is the load along the radial direction of the pivot. For the rocker-backed pad a contact between an outer (pad) and an inner (bearing housing) cylinders is considered, where the length of the contact is equal to L_P = 39.5 mm. For the spherical pivot, the contact between a sphere and a flat surface is considered.

However, in order to validate the model, also the pivot stiffness for each pad of TPJB needs to be identified by experimental activities.

In the initial step for the test, a sufficiently high static load is applied in the middle of the shaft in the vertical direction to make the shaft in contact with the pad. The static load and the corresponding position of the shaft and the pad can be considered as a reference one. In order to obtain more accurate results, the tests are performed in a dry condition to avoid any possible effect of the oil.

The static load is then increased from the reference load up to 3.5 kN, in steps of 0.5 kN. The actual static load applied on the rotor bearing system and the relative displacement of the shaft with respect to the bearing is recorded using two load cells and two proximity probes. As mentioned before, owing to the installation configuration of the hydraulic actuators, the static load can be applied in any directions. The same procedure is applied for all the pads by varying the load direction (see Fig. 5): -90° (LOP pad #1), -18° (LOP pad #2), 54° (LOP pad #3), 126° (LOP pad #4) and 198° (LOP pad #5).

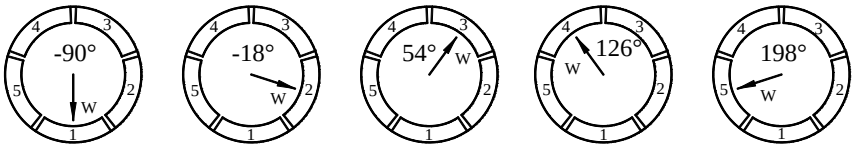

Fig. 5. Varying load configurations.

The local pivot stiffness is the slope of the load versus the displacement fitting curve and can be calculated by:

$$k_{\text{pivot}}^{\text{experiment}} = \frac{\partial F}{\partial X} \tag{4}$$

where ∂F is the increment of applied static load and ∂X is the pivot radial deflection.

This procedure is repeated to calculate the pivot stiffness for the spherical pivot TPJBs. These pivot stiffness values are then introduced in the numerical model for the bearing static as well as dynamic characteristics prediction.

For easy of visualization, Fig. 6 shows the pivot stiffness obtained using the Hertz contact theory and only the identified pivot stiffness of pad #1 of two bearings using the experimental tests.

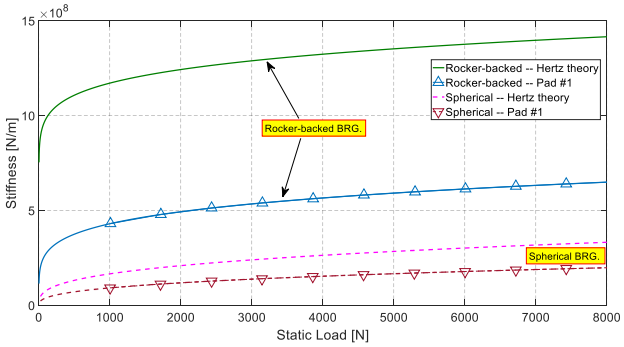

Fig. 6. Pivot stiffness of pad #1 of rocker-backed and spherical pivot TPJB obtained by using the Hertz contact theory and experimental data.

5 Results and discussions

The dynamic stiffness and damping coefficients as functions of applied static load of the rocker-backed and spherical pivot bearing are shown in Fig. 7 and Fig. 8, respectively. All the tests were carried out with the rotational speed of 22 Hz and the force excitation frequency of 25 Hz. In this manner, a quasi-synchronous excitation was supposed. The static load applied in the bearing increased from 2.5 kN to 8.75 kN. The amplitude of dynamic load was chosen approximately 10% of static load in order to avoid nonlinearities of the rotor bearing system.

From Fig. 7 and Fig. 8, it is clear that the direct stiffness coefficients of two bearings increase with the increase of the static load, in which the coefficients in the loaded direction k_{yy} increase at a rate much greater than those in the unloaded direction, k_{xx}. Note that the k_{yy} of two bearings increase significantly approximately two times when the applied static load increases from 2.5 kN to 8.75 kN. Cross-coupled stiffness coefficients are much smaller than the direct coefficients and are of the same sign (positive sign) for k_{yx} and opposite sign (negative sign) for k_{xy}. However, these coefficients are quite stable with excitation frequency and their values can be considered as zero.

In contrast, the measured damping coefficients of two bearings are found to be quite independent with the applied static load, except for the damping coefficient in the loaded direction of the spherical pivot bearing, c_{yy}. It decreases dramatically ap-

proximately 200%, from about 3.8×10^5 N-s/m to about 0.2×10^5 N-s/m in the considered range of applied static load.

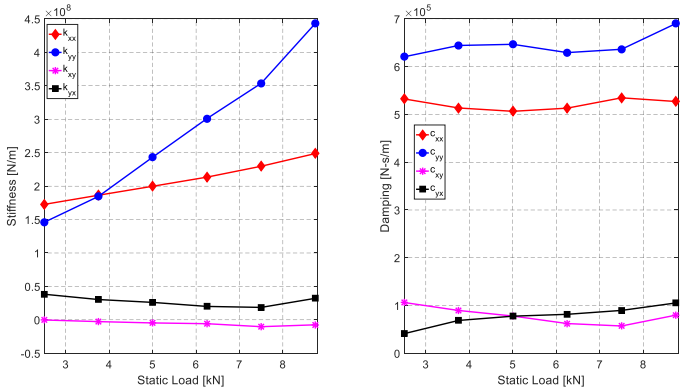

Fig. 7. Experimental dynamic coefficients vs. static load (rocker-backed bearing)

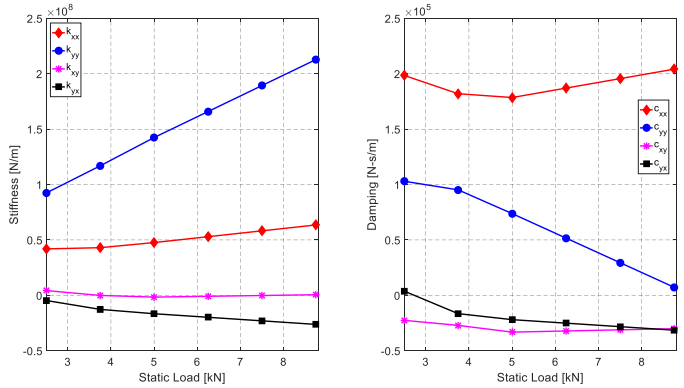

Fig. 8. Experimental dynamic coefficients vs. static load (spherical pivot bearing)

The predicted (solid line) and measured (dashed line) stiffness and damping coefficients of the rocker-backed TPJB are shown in Fig. 9a and Fig. 9b, respectively. The predicted results using the Hertz contact theory and experiment measurements for the pivot stiffness are plotted as well.

The model based on the Hertz contact theory correctly predicts the trend of increasing stiffness coefficients in the unloaded direction, k_{xx} , with the increase of static load. However, this model overestimates k_{xx} approximately 80% that obtained by experiments. Conversely, by using the experimental pivot stiffness, the predicted coefficient k_{xx} shows very good agreement with measured result.

For the stiffness coefficient in the loaded direction, k_{yy} ,the predicted result shows a better agreement with the measured one if the model uses the Hertz theory for the pivot stiffness evaluation, especially at low applied static load. Nevertheless, the code always underestimates the value of k_{yy} approximately 10% and 50% at the lowest and largest applied static load, respectively.

In Fig. 9b, the code over predicts the damping coefficients around 300% for the c_{xx} and about 200% for the c_{yy} in the case of using the Hertz theory for the pivot stiffness. The better predicted results can be obtained if the pivot stiffness is identified from experiments. The discrepancy between the prediction and the measurement in this case reduces to about 20%. It is worthy of notice that the pivot stiffness or the pivot flexibility plays a key role in the dynamic coefficients estimation, particularly the damping coefficients.

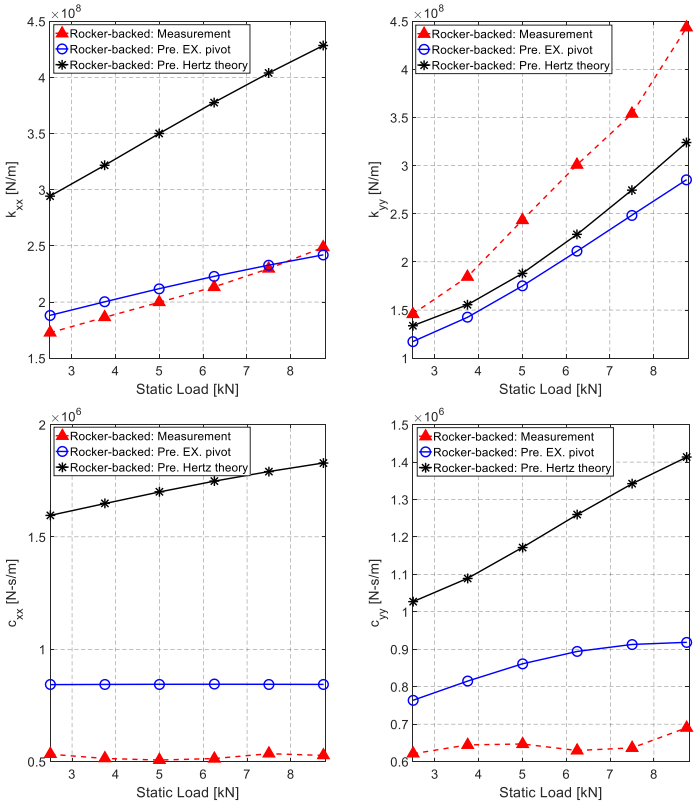

Fig. 9. Rocker-backed bearing: dynamic coefficient vs. static load. Comparison between measurement and prediction.

Fig. 10 represents the comparison between the predicted and measured dynamic coefficients of the spherical pivot bearing as a function of applied static load. It is interesting to note that the results for this bearing are similar to the rocker-backed one. For instance, the predicted coefficient k_{xx} using the experimental pivot stiffness shows very good agreement with measured one. Besides, by using the Hertz contact theory for the pivot stiffness estimation the model correctly predicts the stiffness coefficient in the loaded direction, k_{yy}, especially at low applied static load.

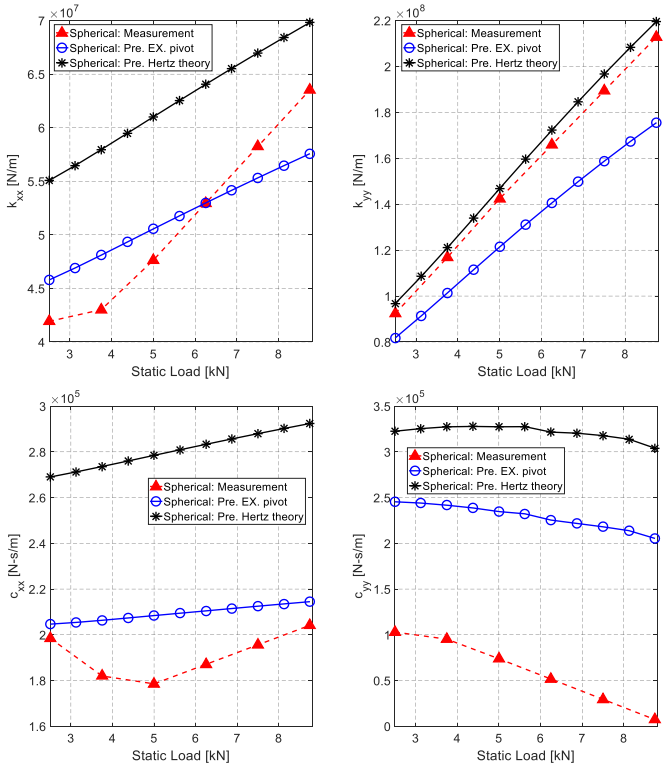

Fig. 10. Spherical pivot bearing: dynamic coefficient vs. static load. Comparison between measurement and prediction

6 Conclusions

In this study, the dynamic characteristics of two different five-shoe TPJBs, namely rocker-backed pivots and spherical pivots with different pivot stiffness were studied using a TEHD model. The experimental tests were performed for these two bearings using a suitable test-rig. The predicted dynamic coefficients of the two tilting-pad bearings were compared with the measured ones. In particular the following conclusions can be drawn:

1. The pivot stiffness values of the spherical pivot pad bearing are approximately one order of magnitude lower than that of the rocker-backed one. In addition, the Hertz contact theory overestimates the pivot stiffness, particularly the rocker-backed bearing.
2. For both bearings, the predicted coefficients in the unloaded direction k_{xx} using the experimental pivot stiffness shows very good agreement with measured ones.
3. It is worthy of notice that the pivot stiffness or the pivot flexibility plays a key role in the estimation of the dynamic coefficients. For both bearings, the predicted coefficients in the unloaded direction k_{xx} using the experimental pivot

stiffness shows very good agreement with measured ones. However, by using the Hertz contact theory for the pivot stiffness estimation the model correctly predicts the stiffness coefficient in the loaded direction, k_{yx}, especially at low applied static load.

4. Regarding the excitation, the more flexible the pad pivot, the lower the dynamic stiffness and damping coefficients, especially the damping coefficients

References

1. Chen, S., Yang, S., Zhou, Q., Hou, Y., Lai, T.: Numerical study on tilting pad journal gas bearing with variable stiffness springs. In Journal of Mechanical Science and Technology, 29(8), 3059-3067 (2015).
2. San Andres L., Tao, Y.: The role of pivot stiffness on the dynamic force coefficients of tilting pad journal bearings. In Journal of Engineering for Gas Turbines and Power, 135(11) (2013).
3. Wilkes, J.C., Childs, D.W.: Tilting pad journal bearing - a discussion on stability calculation, frequency dependence, and pad and pivot. In Journal of Engineering for Gas Turbines and Power, 134(12), 122508 (2015).
4. Feng, K., Liu, W., Zhang, Z., Zhang, T.: Theoretical model of flexure pivot tilting pad gas bearings with metal mesh dampers in parallel. In Tribology International, 94, 26-38 (2016).
5. Cha, M., Glavatskih, S.: Nonlinear dynamic behaviour of vertical and horizontal rotors in compliant liner tilting pad journal bearings: some design considerations. In Tribology International, 82, 142-152 (2015).
6. Kuznetsov, E., Glavatskih, S.: Dynamic characteristics of compliant journal bearings considering thermal effects. In Tribology International, 94, 288-305 (2016).
7. Dang, P.V., Chatterton, S., Pennacchi, P., Vania, A.: Effect of the load direction on non-nominal five-pad tilting-pad journal bearings. In Tribology International, 98, 197-211 (2016).
8. Dang, P.V., Chatterton, S., Pennacchi, P., Vania, A.: Numerical investigation of the effect of manufacturing errors in pads on the behaviour of tilting-pad journal bearings. In Proceedings of the Institution of Mechanical Engineers, Part J: Journal of Engineering Tribology, 233(4), 480-500 (2018).
9. Dang, P.V., Chatterton, S., Pennacchi, P., Vania, A., Cangioli, F.: Behavior of a Tilting–Pad Journal Bearing With Different Load Directions, ASME Paper No. DETC2015-46598, 2015; 8. doi:10.1115/DETC2015-46598
10. Dang, P.V., Chatterton, S., Pennacchi, P., Vania, A., Cangioli, F.: Behavior of tilting-pad journal bearings with large machining error on pads. In ASME Turbo Expo, Paper No. GT GT2016-56674 (2016).
11. Chatterton, S., Dang, P.V., Pennacchi, P, Luca, A.D., Flumian, F.: Experimental evidence of a two-axial groove hydrodynamic journal bearing under severe operation conditions. In Tribology International, 109, 416-427 (2017)
12. Chatterton, S., Dang, P.V., Pennacchi, P., Vania, A.: A test rig for evaluating tilting–pad journal bearing characteristics. In 9th International Conference on Rotor Dynamics IFToMM ICORD, Milan, Italy, 921-930 (2014).
13. Kirk, R.G., Reedy, S.W.: Evaluation of pivot stiffness for typical tilting-pad journal bearing designs. In Journal of Vibration and Acoustics, 10, 165-171 (1988).